

SincPD: An Explainable Method based on Sinc Filters to Diagnose Parkinson’s Disease Severity by Gait Cycle Analysis

Armin Salimi-Badr^{1*}, Mahan Veisi¹ and Sadra Berangi¹

^{1*}Faculty of Computer Science and Engineering, Shahid Beheshti University, Tehran, Iran.

*Corresponding author(s). E-mail(s): a_salimibadr@sbu.ac.ir;

Abstract

In this paper, an explainable deep learning-based classifier based on adaptive sinc filters for Parkinson’s Disease diagnosis (PD) along with determining its severity, based on analyzing the gait cycle (SincPD) is presented. Considering the effects of PD on the gait cycle of patients, the proposed method utilizes raw data in the form of vertical Ground Reaction Force (vGRF) measured by wearable sensors placed in soles of subjects’ shoes. The proposed method consists of Sinc layers that model adaptive bandpass filters to extract important frequency-bands in gait cycle of patients along with healthy subjects. Therefore, by considering these frequencies, the reasons behind the classification a person as a patient or healthy can be explained. In this method, after applying some preprocessing processes, a large model equipped with many filters is first trained. Next, to prune the extra units and reach a more explainable and parsimonious structure, the extracted filters are clusters based on their cut-off frequencies using a centroid-based clustering approach. Afterward, the medoids of the extracted clusters are considered as the final filters. Therefore, only 15 bandpass filters for each sensor are derived to classify patients and healthy subjects. Finally, the most effective filters along with the sensors are determined by comparing the energy of each filter encountering patients and healthy subjects.

Keywords: Parkinson’s Disease, SincNet, Explainability, Wearable Sensors, Gait Cycle

1 Introduction

Parkinson’s Disease (PD) is the second most common neurodegenerative disease affecting many elderly individuals worldwide (Salimi-Badr et al, 2023; Liu et al, 2021; Khoury et al, 2019; Pan et al, 2012; Goyal et al, 2020). It primarily originates from the loss of dopaminergic neurons in the Substantia Nigra pars Compacta within the Basal Ganglia (Hall and Hall, 2020; Salimi-Badr et al, 2017, 2018).

PD treatment typically begins after symptoms manifest years post-infection, necessitating more complex treatments like Deep Brain Stimulus (DBP) instead of simpler lifestyle changes. Early

diagnosis can enable more effective and economical treatments. However, diagnosis is a challenging task that prompts the use of machine learning to enhance healthcare diagnostics.

PD patients often exhibit movement issues such as Bradykinesia, Akinesia, stiffness, and resting tremor (Hall and Hall, 2020). Consequently, machine learning methods focus on movement analysis for diagnosis, including *speech disorders* (Kuresan et al, 2021; Pramanik et al, 2022; Yousif et al, 2023; Liu et al, 2022), *gait changes* (Khoury et al, 2018; Salimi-Badr and Hashemi, 2020; El Maachi et al, 2020; Balaji et al, 2021; Salimi-Badr and Hashemi, 2023; Liu et al, 2021), *handwritten records* (Yousif et al, 2023), *typing speed*

(Prashanth et al, 2016), eye movement changes (Farashi, 2021), multi-modal biomedical time-series analysis (Junaid et al, 2023), and postural stability assessment using RGB-Depth cameras (Ferraris et al, 2024).

Machine Learning, particularly Deep Learning, has been effectively applied in medical diagnosis (El Maachi et al, 2020; Zhao et al, 2018b; Liu et al, 2021). Explainable methods like neuro-fuzzy systems (Salimi-Badr et al, 2023) are limited by their reliance on high-level clinical features. Deep models extract complex features but lack interpretability (Gunning et al, 2019; Hung et al, 2022a). However, explainability is crucial in medical applications to support expert diagnosis (Junaid et al, 2023; Saadatinia and Salimi-Badr, 2024).

Convolutional Neural Networks (CNNs) extract abstract features through learned filters. The first convolutional layers are critical as they process raw signals and form higher-level features. *SincNet* (Ravanelli and Bengio, 2018b) enhances interpretability by using sinc-shaped bandpass filters with only two parameters: center and width. This allows identification of important frequency bands influencing network decisions (Hung et al, 2022b; Ravanelli and Bengio, 2018a).

This paper presents an explainable AI approach to detect PD and assess its severity using sinc-layers in CNNs to analyze vertical-Ground Reaction Force (vGRF) signals from wearable sensors (SincPD). The Sinc layers model adaptive bandpass filters to extract key frequency bands in gait cycles, enabling interpretation of the network's decisions.

Our SincPD involves preprocessing, training a large filter-rich model, pruning redundant filters via centroid-based clustering, and selecting cluster medoids as final filters. We analyze important frequencies by calculating filter energy for patients and healthy subjects.

The paper is organized as follows: Section 2 reviews related machine learning studies for PD detection. Section 3 presents preliminaries. Section 4 details the proposed methodology, including preprocessing, SincNet architecture, learning, and pruning. Section 5 discusses experimental results and filter analysis. Conclusions are in Section 6.

2 Related Work

Parkinson's Disease (PD) is a progressive neurodegenerative disorder marked by motor symptoms (e.g., tremors, rigidity) and non-motor manifestations. Due to the movement disorders, gait analysis has been one of the most popular approaches to study the Parkinson's disease in the literature.

Gait analysis has proven valuable for PD diagnosis due to its ability to identify changes such as reduced stride length, slower speed, and increased variability. Pistacchi et al (2017) observed significant differences in cadence, stride and stance duration, and gait velocity in early-stage PD patients compared to controls. Sofuwa et al (2005) reported shorter step length and slower walking speed, while Lescano et al (2016) found deviations in stance and swing phases and ground reaction force at Hoehn and Yahr stages 2–2.5.

Numerous sensor-based systems have been developed for automated PD detection via gait analysis, extensively utilizing vGRF captured by in-shoe sensors (El Maachi et al, 2020; Balaji et al, 2021; Salimi-Badr and Hashemi, 2023; Vidya B. and Sasikumar P., 2021; Balaji et al, 2020; Zhao et al, 2018b; Liu et al, 2021). Vidya B. and Sasikumar P. (2021) employed spatiotemporal features with a multi-class support vector machine. Salimi-Badr et al (2023) presented a type-2 fuzzy logic approach using vGRF data. and El Maachi et al (2020) proposed a 1D convolutional neural network for PD detection and severity estimation. Zhao et al (2018a) utilized a dual-channel LSTM for gait classification, though limited by partial gait acquisition. Balaji et al (2021) applied LSTM networks for PD diagnosis and severity rating without hand-crafted features, and Vidya B. and Sasikumar P. (2022) introduced a CNN-LSTM model based on empirical mode decomposition of vGRF signals.

Although these machine learning methods have advanced PD diagnosis, many depend on hand-crafted features or lack interpretability. To overcome these limitations, we propose an explainable deep learning model using Sinc filters in a convolutional neural network (CNN) to extract salient frequency bands from raw vGRF data. This approach combines high classification accuracy with transparency, improving the clinical relevance of PD diagnosis and severity assessment.

3 Preliminaries

In this section, we review the preliminaries of the proposed method, including the concept of bandpass filters along with the neural architecture based on them (SincNet).

SincNet Model Architecture. SincNet introduces a novel approach by incorporating parameterized sinc functions into a convolutional neural network (CNN) architecture to efficiently create bandpass filters. This method allows SincNet to learn from only two parameters per filter—lower and upper cutoff frequencies f_1 and f_2 —significantly reducing model complexity.

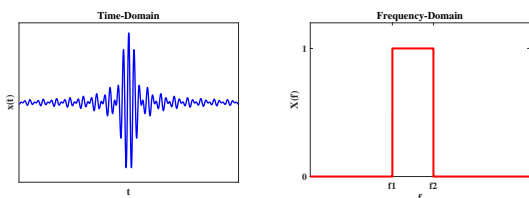


Fig. 1: The impulse-response along with the frequency-response of a bandpass filter that allows selective frequency passage from f_1 to f_2 .

Bandpass Filter Configuration. In SincNet, each filter's impulse response is modeled by the difference between two scaled sinc functions, representing a bandpass filter (Ravanelli and Bengio, 2018b):

$$h[n] = 2f_2 \cdot \text{sinc}(2\pi f_2 n) - 2f_1 \cdot \text{sinc}(2\pi f_1 n), \quad (1)$$

where the sinc function is defined as follows:

$$\text{sinc}(\omega) = \begin{cases} \frac{\sin(\omega)}{\omega} & \text{if } \omega \neq 0, \\ 1 & \text{if } \omega = 0. \end{cases} \quad (2)$$

This impulse response $h[n]$ allows selective frequency passage from f_1 to f_2 , effectively attenuating frequencies outside this range. The form of a sample of this impulse response along with its frequency response is presented in Fig. 1. The design is inspired by the properties of sinc, which acts as an ideal mathematical model for bandpass filters due to its sharp frequency domain characteristics.

Frequency-Domain Characterization. The frequency response of the bandpass filter designed

by SincNet is fundamentally a rectangular function (see Fig. 1), characterized as:

$$G(f) = \text{rect}\left(\frac{f}{2f_2}\right) - \text{rect}\left(\frac{f}{2f_1}\right), \quad (3)$$

where $\text{rect}(\cdot)$ is the rectangular function. The equivalent time-domain representation is shown in Equation (4), illustrating how the sinc functions are used to implement bandpass behavior. The filters are initialized to cover a range of frequencies between 0 and half the sampling rate ($f_s/2$), guided by psychoacoustic principles such as the equivalent rectangular bandwidth (ERB), which aids in setting the filters' bandwidth more precisely.

4 Materials and Methods

In this section, we detail the methodology employed in our study, encompassing the preprocessing steps, the architecture of the proposed deep learning model, and the pruning process.

4.1 Preprocessing

The preprocessing stage ensures input data quality and suitability for the neural network. We prepared the dataset by partitioning it into ten-second segments, filtering out incomplete or inconsistent data, and standardizing the signals. This process ensured clean and normalized inputs for further analysis.

To reduce dimensionality without data loss, we calculated the difference between left and right sensor signals. This approach reduced 16 arrays per subject to 8, effectively preserving critical gait patterns while capturing meaningful inter-sensor variations.

Moreover, stratified splitting was employed to maintain class balance in the training and test datasets, ensuring robustness across patient and healthy subject categories. In summary, Fig. 2 demonstrates an overview of the preprocessing pipeline, including chunking, cleaning, and standardization steps.

4.2 Proposed Architecture

The initial model architecture, depicted in Fig. 3, is designed to efficiently extract and refine meaningful features from vGRF data using a sequential

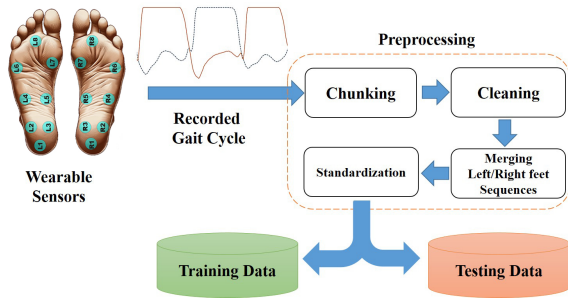


Fig. 2: Overview of the preprocessing pipeline.

framework. Traditional convolutional layers, while powerful for feature extraction, often require a high number of learnable parameters and lack mathematical interpretability, making them less suitable for tasks prioritizing explainability and efficiency.

To address these challenges, the first layers of our model utilize SincConv1D filters. These filters are particularly effective in capturing critical low-level features essential for subsequent processing while maintaining interpretability due to their frequency domain meaning (adaptive bandpass filters). Each filter is parameterized by only two learnable parameters (cutoff frequencies), reducing model complexity and allowing direct analysis of the learned frequency bands. The subsequent layers and their configurations, described in this section, refine these features into robust predictive insights.

4.2.1 SincConv1D Layers

We employ eight SincConv1D layers (one per pre-processed signal) to extract frequency-specific features from vGRF data. In the initial version of the model, each layer is configured with 100 filters of length 101. The extracted features are normalized, activated with Leaky ReLU, and pooled to reduce computational load. Finally, all eight outputs are concatenated, forming a unified representation for subsequent network layers.

4.2.2 Model Structure

Following the frequency-focused SincConv1D feature extraction, two standard Conv1D layers (128 and 256 filters) further refine the learned representations. These layers are followed by Batch Normalization, Leaky ReLU, Dropout, and Max

Pooling to improve model generalization and computational efficiency.

The outputs are then flattened and passed through three Dense layers, with 128, 64, and 1 neuron(s), respectively. The first two layers use ReLU activation, while the final layer employs a sigmoid activation function to output a probability score between 0 and 1. Batch Normalization and L2 regularization are applied to enhance stability and reduce overfitting. Finally, the Adam optimizer (Kingma and Ba, 2015) is applied to learn model's parameters by minimizing the cross-entropy.

4.3 Pruning Method

High number of filters decreases the interpretability. Therefore, we propose a pruning method to prune extra filters. To realize this, we cluster filters based on their cut-off frequencies and reconstruct the architecture based on the clusters' centroids.

As previously described 3, SincConv1D layers learn the center frequency (f_c) and bandwidth (b) of sinc filters, which define their frequency response. These parameters are used for clustering and identifying redundancy. Using K-means clustering (Lloyd, 1982), we group similar (f_c, b) parameters and retain only the most significant clusters.

To determine the optimal number of clusters, we apply the elbow method and silhouette scores (Géron, 2022), initially optimizing for Sensor 1. For each sensor, the optimal k value is identified by analyzing silhouette diagrams for Sinc layers. The clusters and centroids are then visualized to ensure the retained filters capture critical patterns.

The new architecture is constructed using the cluster centroids as filter weights in the SincConv1D layers, reducing parameters while preserving essential patterns. The model is retrained for a few epochs to fine-tune performance, with the rest of the architecture unchanged.

5 Experimental Results

In this section, the performance of the proposed method is evaluated and compared to some previous methods in both diagnosis and severity determination. All experiments have been conducted in CoLab runtime environment based on

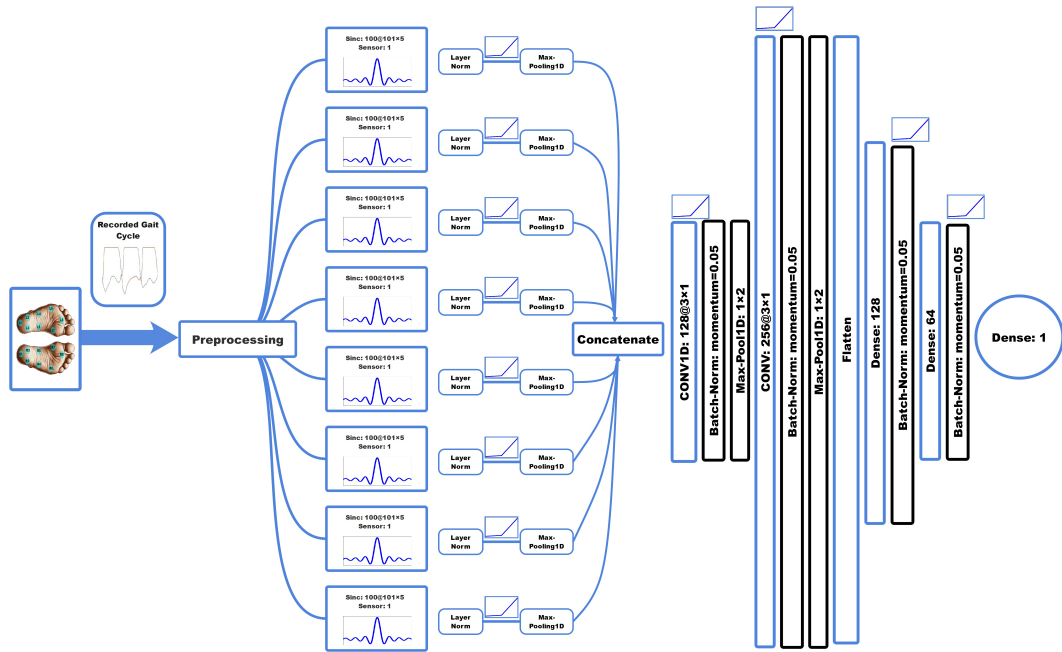


Fig. 3: Architecture of the SincPD. The model begins with an input layer followed by SincConv1D layers, specialized for handling 1D signals. These layers are normalized and activated using the Leaky ReLU function. Following the SincConv1D layers, traditional convolutional layers with batch normalization extract higher-level features. Finally, dense layers are utilized for classification.

Python, using the TensorFlow platform along with the SKLearn package.

5.1 Data and Evaluation Metrics

This study employs gait cycle data from PhysioNet¹, comprising vGRF signals recorded via 16 sensors under participants' feet. The dataset includes individuals with PD and healthy controls, capturing approximately two minutes of walking at a self-selected pace. Gait cycles (Fig. 4), divided into stance and swing phases, highlight PD-related alterations in stride length and variability.

A total of 166 subjects (93 PD, 73 controls) participated, with data aggregated from three separate studies (Table 1). PD severity was assessed based on the modified Hoehn and Yahr scale (Table 2), ranging from Stage 1 (unilateral involvement) to Stage 5 (complete disability).

To evaluate the proposed approach, standard classification metrics including Accuracy, Precision, Recall, and F1 Score were employed.

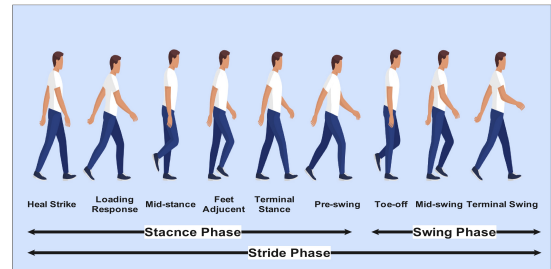


Fig. 4: Illustration of the gait cycle phases. The gait cycle consists of the stance phase (heel strike, loading response, mid-stance, terminal stance, pre-swing includes 60% of the cycle) and the swing phase (toe-off, mid-swing, terminal swing include 40% of the cycle).

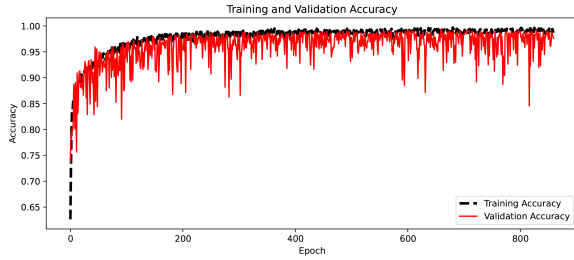
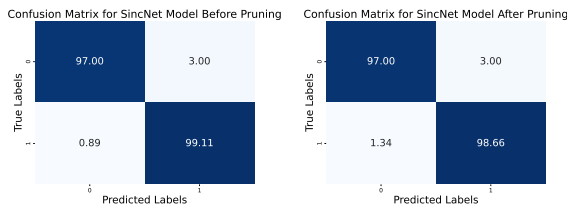
Table 1: Number of participants in datasets categorized by severity level.

| Dataset | Healthy | Stage 2 | Stage 2.5 | Stage 3 |
|---------|---------|---------|-----------|---------|
| Ga | 18 | 15 | 8 | 6 |
| Ju | 26 | 12 | 13 | 4 |
| Si | 29 | 29 | 6 | 0 |

¹<https://physionet.org/content/gaitpdb/1.0.0/>

Table 2: PD severity classification based on the modified H&Y scale.

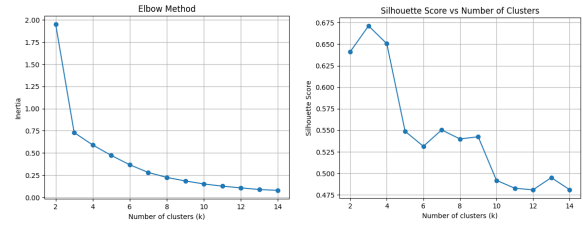
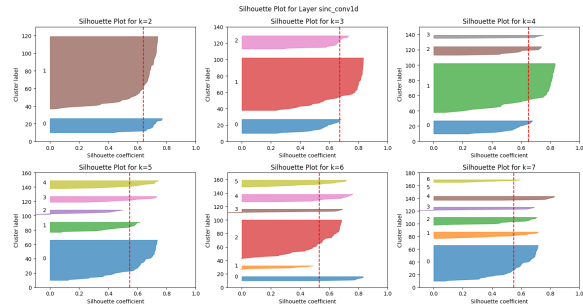
| Scale | Description | Stage |
|-------|---------------------------------------|----------------------------|
| 1 | One side only | No functional disability |
| 1.5 | One side + axial symptoms | Early stage |
| 2 | Bilateral involvement | No balance impairment |
| 2.5 | Mild bilateral, recovery on pull test | Balance impairment |
| 3 | Mild/moderate bilateral | Impaired postural reflexes |
| 4 | Severe disability | Still capable of walking |
| 5 | Bedridden or wheelchair-bound | Completely disabled |

**Fig. 5:** Training and validation accuracy progression over 1000 epochs**Fig. 6:** Confusion matrices: Left, classification performance before pruning; Right, classification performance after pruning.

5.2 Training the Initial Model

The explained model in section 4 is built and trained using the preprocessed data for 1000 epochs. Training and validation accuracy progression (Fig. 5) shows steady improvement, demonstrating effective learning and reliable generalization.

The performance of the trained SincNet model for binary classification is illustrated through a confusion matrix (Fig. 6). The model achieves a high classification accuracy, correctly predicting 97% of samples belong to the negative class and 99.55% of the positive ones, with minimal misclassifications.

**Fig. 7:** Left: Inertia plot for Sensor 1, using the elbow method to suggest an initial cluster range. Right: Silhouette scores for Sensor 1, peaking around $k = 4$, confirming well-separated clusters.**Fig. 8:** Silhouette Diagram for Sensor 1, visually representing cluster cohesion and separation at the optimal k .

5.3 Filter Optimization

To optimize the number of filters in the Sinc-Conv1D layers, we utilize the elbow method and silhouette scores, as described in Section 4.1, to estimate an initial range for the optimal number of clusters.

From the analysis of the plots sampled for Sensor 1 (Fig. 7), the elbow method indicates a potential range of 3 to 7 clusters, while the silhouette scores peak around $k = 4$. These observations suggest that the optimal number of filters lies within this range, which should be refined and evaluated for each sensor individually. Thus, we analyze the optimal k using the silhouette diagram for each sensor. As shown in Fig. 8, the silhouette plots for Sensor 1 suggest $k = 3$ as the best choice, providing optimal cluster cohesion and separation. Repeating this procedure for each sensor yields an efficient clustering configuration, improving the overall filter performance.

For two sample sensors (Sensor 1 and Sensor 5), scatter plots illustrate the distribution of filter

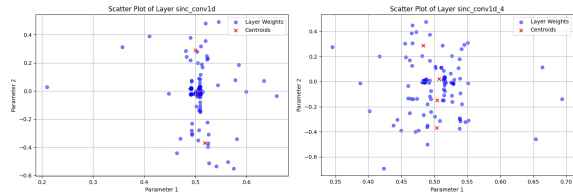


Fig. 9: Scatter plots for two sample sensors (Sensor 1 and Sensor 5), showing clustered filters and their centroids post-clustering. The x-axis represents the bandwidth parameter (b) and the y-axis represents the center frequency parameter (f_c).

weights and their centroids after clustering. For Sensor 1, the Silhouette Diagram analysis determined $k = 3$, and the corresponding centroids were obtained using the k-means algorithm. Similarly, for Sensor 5, $k = 4$ was identified as optimal, resulting in four centroid pairs of (f_c, b) . Fig. 9 displays these clustered filters and centroids.

As described in Section 3, after retraining the model with the pruned filters, the updated architecture maintains nearly the same classification performance as the initial model, despite using significantly fewer SincNet filters. The confusion matrix (Fig. 6, right) shows that the model retains 97% accuracy for the negative class while experiencing only a minor decrease in accuracy for the positive class, from 99.55% to 98.66%.

This minimal reduction in performance is achieved while reducing the total number of filters across the SincNet layers from 800 to approximately 30, significantly decreasing the parameters in the feature extraction layers.

After retraining the pruned model, the preserved filters reveal key insights into the feature extraction process. Fig. 10 illustrates the trained Sinc filters for sensors numbered 5 to 8. These filters reflect the optimized cluster sizes determined during pruning, resulting in a varying number of filters per layer.

The top row of Fig. 10 displays the time-domain representations of the learned Sinc filters, while the bottom row shows their corresponding frequency responses. These frequency bands reveal how the pruned filters capture distinct features relevant to distinguishing healthy and patient signals.

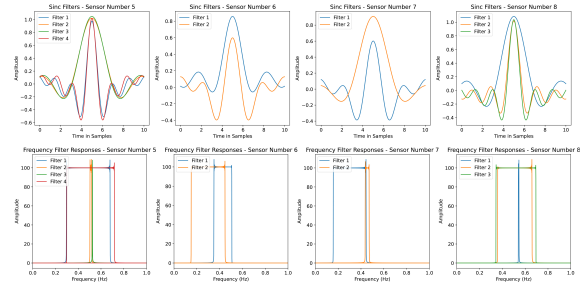


Fig. 10: Visualization of Sinc Filters in Different Layers In Time (First Row) and Frequency (Second Row) Domain

5.4 Effect of filters and sensors

After training the pruned model, we focus on interpreting the feature extraction process within the SincNet layers. By studying the energy distributions of the signals passing through these layers, we aim to uncover how the model distinguishes between healthy and patient signals. This analysis emphasizes the role of the pruned Sinc filters as high-level feature extractors, effectively capturing critical frequency-based patterns for classification.

We aim to calculate the signal energy from the outputs of the pruned SincNet layers, treating these as abstract processed representations of the input signals. This enables us to identify key distinctions in energy patterns between the two classes, offering insights into the discriminatory power of the filters and sensors.

Initially, we seek to identify representative signals for patient and healthy classes. One intuitive approach is to compute the mean signal energy for each class. However, using the mean of all signals may incorporate noise, resulting in similar energy distributions for both classes. This similarity can obscure the distinctions necessary to identify significant sensors and critical signals that enhance classification accuracy. To address this issue, we employ clustering methods such as DBSCAN (Hahsler et al, 2019) to identify core signals that effectively represent each class.

By employing DBSCAN and focusing on clusters, we identify the most representative real samples of healthy and patient signals. These clusters serve as class representatives, enabling accurate evaluation of energy distributions and highlighting key differences between PD and

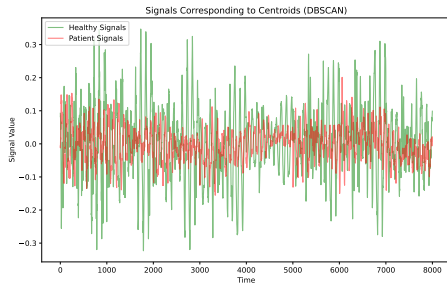


Fig. 11: DBSCAN centroids representing healthy and patient signals.

healthy signals. Fig. 11 depicts the centroids obtained using DBSCAN clustering.

Once the representative signals for patient and healthy classes are identified, they are passed through the pruned SincNet layers to analyze the output energy distributions. This analysis helps determine which specific filters within each sensor are most significant for distinguishing between the two classes. For example, in Sensor 1 (top-left corner of Fig. 12), the output energies of the first, second, and fourth filters exhibit noticeable differences between healthy and patient signals. These differences suggest that the corresponding Sinc filters are targeting specific frequency ranges crucial for classification. To systematically identify such impactful filters, we calculate the difference in output energy between healthy and patient signals across all filters of the eight sensors.

As illustrated in Fig. 12 (second row), the corresponding differences in output energy values for two sample sensors (Sensor 1 and Sensor 4) are shown, highlighting some filters with notable variations between the two classes.

We then analyze the distribution of these energy differences across all sensors and their pruned filters to identify the discriminatory power of individual filters and sensors. Fig. 13 illustrates the distribution of energy differences for all sensors and filters. From this analysis, we observe that certain sensors and filters exhibit larger energy differences, making them critical for further investigation. To better understand the characteristics of these impactful filters, we focus on analyzing the top 20% based on their energy difference metric. These filters could provide valuable information for understanding the mechanisms of the model's decision-making process, likely capturing

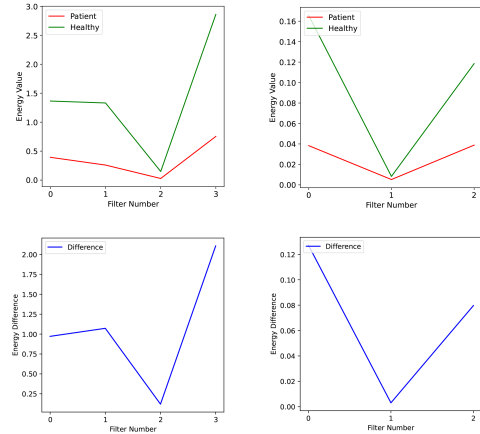


Fig. 12: Energy distribution for patient and healthy signals using centroids for two sample sensors (Sensor 1 and Sensor 4, first row) and the corresponding differences in energy values across filters (second row).

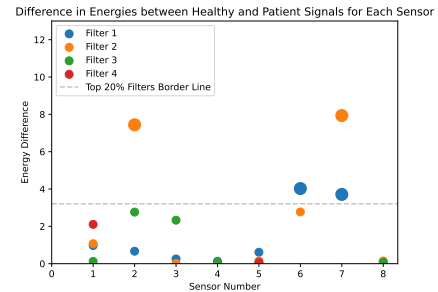


Fig. 13: Distribution of Energy Differences Across Sensors and Filters

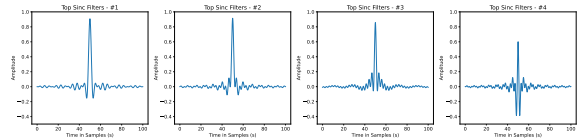


Fig. 14: Top Filters Based on Energy Differences (Time Domain)

crucial features for distinguishing between healthy and patient signals.

Fig. 14 and Fig. 15 display the top filters identified in the time and frequency domains, respectively. From Fig. 15, the first two top filters, primarily associated with Sensor 7 (ball of the foot) and Sensor 2 (heel), as indicated in

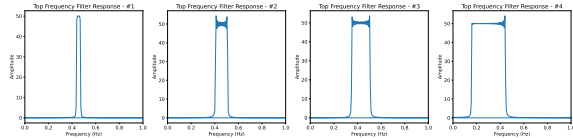


Fig. 15: Top Filters Based on Energy Differences (Frequency Domain)

Fig.2 for sensor locations, focus on bandpassing frequencies in the range of approximately 0.4 to 0.6 Hz while attenuating other frequencies. Similarly, the fourth filter, derived from Sensor 7, targets a narrower band of 0.2 to 0.5 Hz. These frequency ranges highlight filter selectivity in targeting class-specific features, underlining their role in distinguishing between healthy and patient gait signals.

Furthermore, based on Fig. 13, sensors positioned at the front (e.g., Sensors 6 and 7) and back (e.g., Sensors 1 to 3) of the foot demonstrate higher energy differences. This suggests that these regions contribute more prominently to the model’s feature extraction process, potentially due to their biomechanical significance in gait patterns.

5.5 Severity Model Integration

We integrate the severity model for Parkinson’s disease into our framework using transfer learning. A pretrained cluster model, obtained via the pruning method described in Section 3.5, provides the initial weights for the severity model. To preserve learned representations, we freeze the clustered model’s layers and align the severity model’s layers to these pre-trained weights. This setup leverages the feature extraction capabilities already established by the clustered model.

After initialization, the severity model undergoes further training or evaluation to classify PD severity levels. It achieves a 97.22% accuracy in multi-class classification. The confusion matrix for these severity predictions is shown in Fig. 16.

5.6 Performance Comparison

Our proposed model demonstrates superior performance in both binary and multi-class classification tasks compared to state-of-the-art methods, as summarized in Tables 3 and 4.

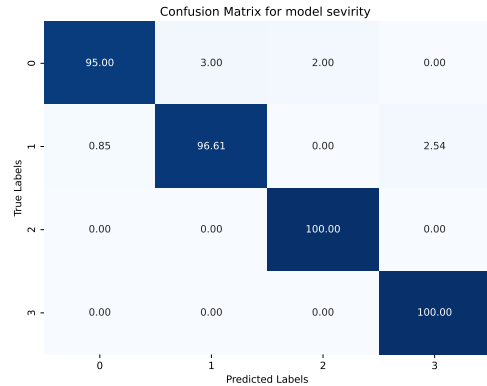


Fig. 16: Confusion matrix for severity model

Table 3: Model Performance Comparison Before and After Pruning State of Art Methods for Binary Classification

| Method | Acc (%) | Prec (%) | Recall (%) | F1 (%) | Params |
|--|--------------|--------------|--------------|--------------|-------------|
| LSTM ¹ | 98.60 | 98.23 | 96.6 | 98.95 | 1.12M |
| Multi LSTM ² | 91.95 | 88.75 | 96.66 | 92.53 | 33.86K |
| CNN+LSTM ³ | 98.09 | 99.22 | 100 | 98.04 | 89.2M |
| ResNet-101 ⁴ | 97.56 | - | 97.73 | - | 44.5M |
| SincPD <i>Before Pruning</i> | 98.77 | 98.67 | 99.55 | 99.11 | 1.17M |
| SincPD <i>After Pruning</i> | 98.15 | 98.66 | 98.66 | 98.66 | 872K |

Table 4: Comparison of Model Performance with State of Art Deep Learning Methods for Multi-Classification

| Method | Acc (%) | Prec (%) | Recall (%) | F1 (%) |
|----------------------|--------------|--------------|--------------|--------------|
| 1D CNN ⁵ | 85.23 | 87.30 | 85.3 | 85.3 |
| LSTM ² | 96.60 | 98.70 | 96.20 | 97.43 |
| ANN-FFT ⁶ | 97.00 | 98.00 | 94.00 | 96.00 |
| SincPD | 97.22 | 97.30 | 97.22 | 97.24 |

Tables 3 and 4 illustrate that the proposed model outperforms existing state-of-the-art methods in both binary and multi-class classification tasks. For binary classification, it achieves an accuracy of 98.77% before pruning and maintains 98.15% post-pruning with only 872K parameters, surpassing model like LSTM in both performance and efficiency. In multi-class classification, the model attains a 97.22% accuracy, which is competitive with top methods such as LSTM and LSTM-CNN combinations. Additionally, the proposed model offers enhanced explainability compared to existing approaches. These results demonstrate

¹* ¹ (Balaji et al, 2021), ² (Salimi-Badr and Hashemi, 2023), ³ (Liu et al, 2021), ⁴ (Setiawan and Lin, 2021), ⁵ (El Maachi et al, 2020), ⁶ (Suquilanda-Pesántez et al, 2021).

the proposed model's superior accuracy, precision, recall, and F1 scores while significantly reducing model complexity, underscoring its effectiveness, scalability, and interpretability in diverse classification scenarios.

6 Conclusions

In this paper an interpretable deep structure is proposed to classify patients with Parkinson's disease and healthy subjects according to their gait cycle pattern. The proposed method can also determine the severity of the disease.

The proposed method is a deep structure that takes the low-level raw vertical Ground Reaction Force (vGRF) signal recorded by 16 sensors put in the subjects' shoes as the input and extract higher level features based on applying various filters. Our proposed method applies bandpass filters with sinc-shape impulse responses in its first layers. Consequently, model is encouraged to learn the main frequencies of each sensor which is various between patients and healthy movements. This extraction leads to extract more meaningful features. These filters have lower number of parameters that make the method a light-weight deep model. Moreover, based on analyzing the active filters during the inference process, the important filters and sensors are determined. This information can be utilized to explain the network's output.

To train the proposed method, first a large model with a lot of filters is trained. Next, the extracted bandpass filters are studied and clustered based on their cut-off frequencies. Based on this clustering, the extra filters are pruned by replacing them with the medoids of the extracted clusters.

The model achieved an accuracy of 98.77% and 98.15% before and after applying the pruning process in PD diagnosis, and an accuracy of 97.22% in severity detection problem. The proposed method outperforms previous models with a more parsimonious structure while providing more explanations on the reasons behind its decisions.

Authors' Contributions **Armin Salimi-Badr:** Conceptualization, Methodology, Formal analysis, Theoretical analysis, Validation, Investigation, Supervision, Writing - original draft, Writing - review & editing, Project administration. **Mahan Veisi** and **Sadra Berangi:** Methodology, Software, Validation, Data curation, Visualization, Writing - original draft.

Funding The is not any funding .

Data Availability The dataset used during the current study is an open access dataset from free public database, available in PhysioNet².

Declarations

Conflict of Interest None.

Ethical Approval Not applicable.

Consent to Participate Not applicable.

Consent for Publication Not applicable.

Clinical Trial Number Not applicable.

References

- Balaji E, Brindha D, R. B (2020) Supervised machine learning based gait classification system for early detection and stage classification of parkinson's disease. *Applied Soft Computing* 94:106494. <https://doi.org/https://doi.org/10.1016/j.asoc.2020.106494>
- Balaji E, Brindha D, Elumalai V, et al (2021) Automatic and non-invasive parkinson's disease diagnosis and severity rating using lstm network. *Applied Soft Computing* 108:107463. <https://doi.org/https://doi.org/10.1016/j.asoc.2021.107463>
- El Maachi I, Bilodeau GA, Bouachir W (2020) Deep 1d-convnet for accurate parkinson disease detection and severity prediction from gait. *Expert Systems with Applications* 143:113075. <https://doi.org/https://doi.org/10.1016/j.eswa.2019.113075>
- Farashi S (2021) Analysis of vertical eye movements in parkinson's disease and its potential for diagnosis. *Applied Intelligence* 51(11):8260–8270. <https://doi.org/10.1007/s10489-021-02364-9>

²<https://physionet.org/content/gaitpdb/1.0.0/>

- Ferraris C, Votta V, Nerino R, et al (2024) At-home assessment of postural stability in parkinson's disease: a vision-based approach. *Journal of Ambient Intelligence and Humanized Computing* 15(5):2765–2778
- Géron A (2022) Hands-on machine learning with Scikit-Learn, Keras, and TensorFlow. ” O'Reilly Media, Inc.”
- Goyal J, Khandnor P, Aseri TC (2020) Classification, prediction, and monitoring of parkinson's disease using computer assisted technologies: A comparative analysis. *Engineering Applications of Artificial Intelligence* 96:103955. <https://doi.org/10.1016/j.engappai.2020.103955>
- Gunning D, Stefik M, Choi J, et al (2019) Xai—explainable artificial intelligence. *Science Robotics* 4(37):eaay7120
- Hahsler M, Piekenbrock M, Doran D (2019) dbSCAN: Fast density-based clustering with R. *Journal of Statistical Software* 91(1):1–30. <https://doi.org/10.18637/jss.v091.i01>
- Hall JE, Hall ME (2020) Guyton and hall textbook of medical physiology, 14th edn. Guyton Physiology, Elsevier - Health Sciences Division, Philadelphia, PA
- Hung CH, Wang SS, Wang CT, et al (2022a) Using sincnet for learning pathological voice disorders. *Sensors* 22(17):6634
- Hung CH, Wang SS, Wang CT, et al (2022b) Using sincnet for learning pathological voice disorders. *Sensors* 22(17):6634
- Junaid M, Ali S, Eid F, et al (2023) Explainable machine learning models based on multimodal time-series data for the early detection of parkinson's disease. *Computer Methods and Programs in Biomedicine* 234:107495. <https://doi.org/10.1016/j.cmpb.2023.107495>
- Khoury N, Attal F, Amirat Y, et al (2018) Cdtw-based classification for parkinson's disease diagnosis. In: ESANN
- Khoury N, Attal F, Amirat Y, et al (2019) Data-driven based approach to aid parkinson's disease diagnosis. *Sensors* 19(2):242
- Kingma DP, Ba J (2015) Adam: A method for stochastic optimization. In: 3rd International Conference on Learning Representations, ICLR 2015, pp 1021–1028, <https://doi.org/10.1109/SLT.2018.8639585>
- Kuresan H, Samiappan D, Ghosh S, et al (2021) Early diagnosis of parkinson's disease based on non-motor symptoms: a descriptive and factor analysis. *Journal of Ambient Intelligence and Humanized Computing* <https://doi.org/10.1007/s12652-021-02944-0>, URL <http://dx.doi.org/10.1007/s12652-021-02944-0>
- Lescano C, Rodrigo S, Christian D (2016) A possible parameter for gait clinimetric evaluation in parkinson's disease patients. In: *Journal of Physics: Conference Series*, IOP Publishing, p 012019
- Liu W, Liu J, Peng T, et al (2022) Prediction of parkinson's disease based on artificial neural networks using speech datasets. *Journal of Ambient Intelligence and Humanized Computing* 14(10):13571–13584. <https://doi.org/10.1007/s12652-022-03825-w>, URL <http://dx.doi.org/10.1007/s12652-022-03825-w>
- Liu X, Li W, Liu Z, et al (2021) A dual-branch model for diagnosis of parkinson's disease based on the independent and joint features of the left and right gait. *Applied Intelligence* 51(10):7221–7232. <https://doi.org/10.1007/s10489-020-02182-5>, URL <https://doi.org/10.1007/s10489-020-02182-5>
- Lloyd S (1982) Least squares quantization in pcm. *IEEE Transactions on Information Theory* 28(2):129–137. <https://doi.org/10.1109/TIT.1982.1056489>
- Pan S, Iplikci S, Warwick K, et al (2012) Parkinson's disease tremor classification—a comparison between support vector machines and neural networks. *Expert Systems with Applications* 39(12):10764–10771
- Pistacchi M, Gioulis M, Sanson F, et al (2017) Gait analysis and clinical correlations in early parkinson's disease. *Functional neurology* 32(1):28
- Pramanik M, Pradhan R, Nandy P, et al (2022) The forex++ based decision tree ensemble approach for robust detection of parkinson's disease. *Journal of Ambient Intelligence and Humanized Computing* 14(9):11429–11453. <https://doi.org/10.1007/s12652-022-03719-x>, URL <http://dx.doi.org/10.1007/s12652-022-03719-x>
- Prashanth R, Roy SD, Mandal PK, et al (2016) High-accuracy detection of early parkinson's disease through multimodal features and

- machine learning. *International journal of medical informatics* 90:13–21
- Ravanelli M, Bengio Y (2018a) Interpretable convolutional filters with sincnet. *arXiv preprint arXiv:181109725*
- Ravanelli M, Bengio Y (2018b) Speaker recognition from raw waveform with sincnet. In: 2018 IEEE Spoken Language Technology Workshop (SLT), pp 1021–1028, <https://doi.org/10.1109/SLT.2018.8639585>
- Saadatinia M, Salimi-Badr A (2024) An explainable deep learning-based method for schizophrenia diagnosis using generative data-augmentation. *IEEE Access* 12:98379–98392. <https://doi.org/10.1109/access.2024.3428847>, URL <http://dx.doi.org/10.1109/ACCESS.2024.3428847>
- Salimi-Badr A, Hashemi M (2020) A neural-based approach to aid early parkinson's disease diagnosis. In: 2020 11th International Conference on Information and Knowledge Technology (IKT), pp 23–25, <https://doi.org/10.1109/IKT51791.2020.9345635>
- Salimi-Badr A, Hashemi M (2023) Early parkinson's disease diagnosis based on sequence analysis. *Journal of Innovations in Computer Science and Engineering (JICSE)* 1(1):1–10. <https://doi.org/10.48308/jicse.2023.103523>
- Salimi-Badr A, Ebadzadeh MM, Darlot C (2017) A possible correlation between the basal ganglia motor function and the inverse kinematics calculation. *Journal of Computational Neuroscience* 43(3):295–318
- Salimi-Badr A, Ebadzadeh MM, Darlot C (2018) A system-level mathematical model of basal ganglia motor-circuit for kinematic planning of arm movements. *Computers in Biology and Medicine* 92:78–89
- Salimi-Badr A, Hashemi M, Saffari H (2023) A type-2 neuro-fuzzy system with a novel learning method for parkinson's disease diagnosis. *Applied Intelligence* 53(12):15656–15682. <https://doi.org/10.1007/s10489-022-04276-8>, URL <https://doi.org/10.1007/s10489-022-04276-8>
- Setiawan F, Lin CW (2021) Implementation of a deep learning algorithm based on vertical ground reaction force time–frequency features for the detection and severity classification of parkinson's disease. *Sensors* 21(15). <https://doi.org/10.3390/s21155207>
- Sofuwa O, Nieuwboer A, Desloovere K, et al (2005) Quantitative gait analysis in parkinson's disease: Comparison with a healthy control group. *Archives of Physical Medicine and Rehabilitation* 86(5):1007–1013. <https://doi.org/https://doi.org/10.1016/j.apmr.2004.08.012>
- Suquilanda-Pesántez JD, Zambonino-Soria MC, López-Ramos DE, et al (2021) Prediction of parkinson's disease severity based on gait signals using a neural network and the fast fourier transform. In: Botto-Tobar M, Cruz H, Díaz Cadena A (eds) *Artificial Intelligence, Computer and Software Engineering Advances*. Springer International Publishing, Cham, pp 3–18
- Vidya B., Sasikumar P. (2021) Gait based parkinson's disease diagnosis and severity rating using multi-class support vector machine. *Applied Soft Computing* 113:107939. <https://doi.org/https://doi.org/10.1016/j.asoc.2021.107939>
- Vidya B., Sasikumar P. (2022) Parkinson's disease diagnosis and stage prediction based on gait signal analysis using emd and cnn-lstm network. *Engineering Applications of Artificial Intelligence* 114:105099. <https://doi.org/https://doi.org/10.1016/j.engappai.2022.105099>
- Yousif NR, Balaha HM, Haikal AY, et al (2023) A generic optimization and learning framework for parkinson disease via speech and handwritten records. *Journal of Ambient Intelligence and Humanized Computing* 14(8):10673–10693
- Zhao A, Qi L, Dong J, et al (2018a) Dual channel lstm based multi-feature extraction in gait for diagnosis of neurodegenerative diseases. *Knowledge-Based Systems* 145:91–97. <https://doi.org/https://doi.org/10.1016/j.knsys.2018.01.004>
- Zhao A, Qi L, Li J, et al (2018b) A hybrid spatio-temporal model for detection and severity rating of parkinson's disease from gait data. *Neurocomputing* 315:1–8. <https://doi.org/https://doi.org/10.1016/j.neucom.2018.03.032>